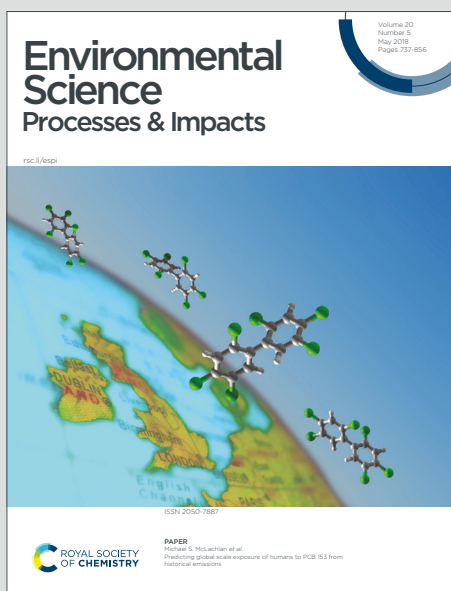


# Environmental Science Processes & Impacts

Accepted Manuscript

This article can be cited before page numbers have been issued, to do this please use: M. J. Berens, G. Schwaner and E. M. Herndon, *Environ. Sci.: Processes Impacts*, 2026, DOI: 10.1039/D6EM00129G.



This is an Accepted Manuscript, which has been through the Royal Society of Chemistry peer review process and has been accepted for publication.

Accepted Manuscripts are published online shortly after acceptance, before technical editing, formatting and proof reading. Using this free service, authors can make their results available to the community, in citable form, before we publish the edited article. We will replace this Accepted Manuscript with the edited and formatted Advance Article as soon as it is available.

You can find more information about Accepted Manuscripts in the [Information for Authors](#).

Please note that technical editing may introduce minor changes to the text and/or graphics, which may alter content. The journal's standard [Terms & Conditions](#) and the [Ethical guidelines](#) still apply. In no event shall the Royal Society of Chemistry be held responsible for any errors or omissions in this Accepted Manuscript or any consequences arising from the use of any information it contains.

**EM-ART-02-2026-000129**

**Environmental Significant Statement**

Emerging freshwater deltas influence the fate of C and nutrients exported from inland waters, with elevation and inundation gradients shaping soil biogeochemical processes. This study clarifies how soil chemical properties and inundation regulate C and P release from emerging deltaic systems. Older soils support greater biogeochemical activity in supratidal and intertidal zones, likely reflecting higher soil C concentrations. Inundation-driven redox oscillations in intertidal zones enhance OM decomposition to CO<sub>2</sub> and accelerate Fe(III) (oxyhydr)oxide turnover, whereas persistent subtidal saturation restricts O<sub>2</sub> availability and inhibits Fe-OC and Fe-P associations, though microbial Fe reduction may sustain OM decomposition and P release under anoxic conditions. This study advances understanding of how hydrogeomorphic development and Fe redox cycling jointly govern C storage and nutrient buffering in active coastal deltas.

1  
2  
3  
4  
5  
6  
7  
8  
9  
10  
11  
12  
13  
14  
15  
16  
17  
18  
19  
20  
21  
22  
23  
24  
25  
26  
27  
28  
29  
30  
31  
32  
33  
34  
35  
36  
37  
38  
39  
40  
41  
42  
43  
44  
45  
46  
47  
48  
49  
50  
51  
52  
53  
54  
55  
56  
57  
58  
59  
60

Open Access Article. Published on 06 May 2026. Downloaded on 5/7/2026 2:46:05 PM.  
This article is licensed under a Creative Commons Attribution-NonCommercial 3.0 Unported Licence.



Environmental Science: Processes & Impacts Accepted Manuscript

## Carbon and nutrient mobilization across inundation gradients in an emerging freshwater delta

Matthew J. Berens,<sup>1,\*</sup> Geoff Schwaner,<sup>1</sup> and Elizabeth M. Herndon<sup>1</sup>

<sup>1</sup>Environmental Sciences Division, Oak Ridge National Laboratory, Oak Ridge, TN 37831

\*corresponding author: [matthew.berens@ncagr.gov](mailto:matthew.berens@ncagr.gov)

<sup>+</sup>Current address: North Carolina Department of Agriculture and Consumer Services, Raleigh, NC 27699

### Abstract (50–250 words)

Emerging freshwater deltas are comprised of gradients of soil age and inundation frequency that influence biogeochemical processes. Differences in inundation patterns coupled with soil chemical properties may affect whether carbon and nutrients transported from inland watersheds are stored in delta soils or released into the atmosphere or open ocean. This study uses laboratory incubations to evaluate the responses of soil, porewater, and headspace parameters to different inundation patterns in soils collected from two elevation transects of an emerging deltaic island in the Wax Lake Delta in Louisiana, USA, an active freshwater delta forming along the Louisiana coast in response to water diversions. In general, soils from the older region of the island exhibited higher CO<sub>2</sub> release and solute mobilization relative to soils from the younger delta region. In addition, persistent inundation was associated with significantly lower solute (DOC, Fe, P) and CO<sub>2</sub> release than soil exposed to persistently drained conditions or periodic flood-drain cycles. Our results indicate that biogeochemical processes, such as organic matter decomposition and microbial Fe cycling, may be limited by inundated conditions in subtidal zones but vary in response to differences in soil chemical properties (e.g., C and N content) across supratidal and intertidal regimes. These results demonstrate that hydrogeomorphic development, in addition to inundation patterns, regulate biogeochemical processes that produce solutes and gases in coastal systems.

**Notice:** This manuscript has been authored by UT-Battelle, LLC, under contract DE-AC05-00OR22725 with the US Department of Energy (DOE). The US government retains and the publisher, by accepting the article for publication, acknowledges that the US government retains a nonexclusive, paid-up, irrevocable, worldwide license to publish or reproduce the published form of this manuscript, or allow others to do so, for US government purposes. DOE will provide public access to these results of federally sponsored research in accordance with the DOE Public Access Plan (<https://www.energy.gov/doe-public-access-plan>).

1  
2  
3  
4  
5  
6  
7  
8  
9  
10  
11  
12  
13  
14  
15  
16  
17  
18  
19  
20  
21  
22  
23  
24  
25  
26  
27  
28  
29  
30  
31  
32  
33  
34  
35  
36  
37  
38  
39  
40  
41  
42  
43  
44  
45  
46  
47  
48  
49  
50  
51  
52  
53  
54  
55  
56  
57  
58  
59  
60

Open Access Article. Published on 06 May 2016. Downloaded on 5/7/2016 2:46:05 PM.  
This article is licensed under a Creative Commons Attribution-NonCommercial 3.0 Unported Licence.



## 36 Introduction

37 Coastal zones contain hydrologically dynamic ecosystems that receive freshwater from inland  
38 watersheds before it is discharged to the ocean. Within coastal ecosystems, interactions between  
39 land, freshwater, and seawater influence the cycling of solutes and particulates, and support key  
40 ecosystem services including carbon storage, nutrient buffering, and mitigation of flooding and  
41 storm surges.<sup>1,2</sup> In many coastal systems, sea level rise and alterations to rivers and streams  
42 (e.g., river impoundment, groundwater extraction, land-use conversion) are causing extensive  
43 inundation and land erosion.<sup>3–5</sup> River diversions are a proposed approach to offset these losses  
44 by directing freshwater and sediment flows towards degrading coastlines to accelerate the vertical  
45 accretion of new land.<sup>6–8</sup> These diversions may alter the biogeochemical conditions of coastal  
46 zones by increasing the supply of carbon, nutrients (i.e., N and P), and iron (Fe) while  
47 simultaneously lowering salinity.<sup>9</sup> An improved understanding of soil biogeochemistry in coastal  
48 ecosystems that are gaining land due to river diversions is critical for determining the impact of  
49 these activities on future carbon and nutrient cycling.

50  
51 Deltas that form in response to river diversions are characterized by freshwater-dominated  
52 channels and a series of aggrading islands that span gradients of time since subaerial emergence  
53 and frequency of inundation.<sup>10,11</sup> Soils at the proximal (upstream) end and along the natural  
54 embankments around the perimeter of the islands are often older, reach higher elevations, and  
55 have higher organic matter content relative to distal (downstream) sedimentation regions and the  
56 inter-distributary bays that comprise the island interiors.<sup>12</sup> The resulting elevation gradients  
57 spanning both upstream to downstream and from exterior to interior of the growing islands yield  
58 distinct hydrogeomorphic zones defined by ground surface elevation relative to the tidal range:  
59 supratidal (primarily drained at the ground surface); intertidal (periodically inundated by tides); or  
60 subtidal (consistently inundated). These zones contain characteristic vegetation ranging from  
61 emergent aquatic plants in subtidal areas (e.g., *Nelumbo lutea*, *Lemma minor*) to wetland forest  
62 and herbaceous wetland species at higher elevations (e.g., *Salix nigra*, *Colocasia esculenta*,  
63 *Polygonum punctatum*).<sup>11,13,14</sup> While several studies have described the sedimentation and  
64 vegetation patterns of emerging deltas, fewer studies have examined the effects of variable  
65 inundation on soil and porewater chemistry across elevation gradients.<sup>15–17</sup>

66  
67 Carbon and nutrient dynamics in coastal systems are strongly influenced by redox-driven  
68 biogeochemical processes. In particular, variable inundation due to (semi-)diurnal tidal cycles  
69 and/or periods of low or elevated river discharge can oscillate soils between oxic and anoxic  
70 conditions, potentially resulting in the formation and/or dissolution of reactive Fe minerals (i.e.,  
71 Fe(III) oxides and oxyhydroxides).<sup>18,19</sup> When oxygen is depleted under flooded conditions, short  
72 range ordered (SRO) Fe(III) oxyhydroxides (e.g., ferrihydrite) may act as terminal electron  
73 acceptors for microbial respiration, promoting the decomposition of organic carbon into  
74 greenhouse gases (i.e., carbon dioxide (CO<sub>2</sub>)).<sup>20</sup> In addition, Fe(III) oxyhydroxides may strongly  
75 adsorb organic matter, nutrients, and trace elements which can then be released into soil  
76 porewaters during reductive mineral dissolution.<sup>21</sup> As soil moisture decreases with receding tides  
77 and/or river stage, soil pore spaces become aerated, causing the oxidative precipitation of  
78 dissolved or complexed Fe(II) into new solid Fe(III) phases. This formation of iron minerals could  
79 potentially stabilize large amounts of carbon and nutrients through adsorption and/or  
80 coprecipitation and increase carbon retention in deltaic soils.<sup>17,18,22–28</sup> While Fe redox cycling is  
81 recognized as a key process in coastal wetlands, its relative importance compared to other factors  
82 (e.g., soil age and composition) in controlling C and nutrient dynamics across inundation gradients  
83 in freshwater deltas remains unclear.

84

1  
2  
3 85 The objectives of this study were to (i) investigate how CO<sub>2</sub> production and solute mobility respond  
4 86 to different inundation conditions across an emerging freshwater delta and (ii) to assess how Fe  
5 87 mineral precipitation and dissolution may affect solute immobilization and release. Surface soils  
6 88 (<30 cm) collected from supratidal, intertidal, and subtidal zones along two elevation transects in  
7 89 the Wax Lake Delta representing different timepoints of island development were incubated in  
8 90 laboratory mesocosms under conditions that reflected those experienced in the field: static  
9 91 drained (supratidal); repeated flood-drain cycles (intertidal); or static inundated (subtidal).<sup>10,11</sup>  
10 92 Mesocosms were assessed for differences in greenhouse gas emissions (CO<sub>2</sub>, CH<sub>4</sub>, N<sub>2</sub>O) and  
11 93 the release of redox-sensitive analytes (DOC, Fe), nutrients (P), and cations (Ca, Mg, Al) into soil  
12 94 porewater. The concentrations of soil Fe contained in SRO and LRO Fe(III) (oxyhydr)oxide  
13 95 minerals were quantified before and after incubation using selective chemical extractions.  
14 96

## 97 **Methods**

### 98 **Site description**

99 The Wax Lake Delta (WLD) is located approximately 30 km southwest of Morgan City in Coastal  
100 Louisiana, USA (Figure 1). This region experiences an annual precipitation of 1,530 mm·yr<sup>-1</sup> and  
101 daily mean temperatures ranging from 12 to 29 °C in winter and summer, respectively.<sup>29</sup> Wax  
102 Lake Delta is an active delta forming from sediments delivered through the Wax Lake Outlet, a  
103 channel constructed in 1941 to reduce flood stages in Coastal Louisiana communities by diverting  
104 a portion of the flow from the Atchafalaya River.<sup>30</sup> The resulting high sediment load (25.6–38.4  
105 Mt·yr<sup>-1</sup>)<sup>31</sup> in the Wax Lake Outlet has created a series of rapidly aggrading islands that initially  
106 became subaerial following a major flood in 1973 and now consist of a range of freshwater  
107 habitats (mean channel salinity 0.11 ± 0.004 ppt)<sup>32</sup> spanning forested wetlands to herbaceous  
108 marshes.  
109

110 Wax Lake Delta exhibits distinct hydrogeomorphic zones defined by soil elevation, water level,  
111 and frequency of inundation.<sup>10,11,33</sup> Supratidal zones of the WLD are above the mean high water  
112 level (>0.3 m NAVD88) and inundated only during seasonal and extreme high-water events.  
113 These areas occur along the natural levees that border the islands and contain early successional  
114 woody vegetation, including black willow (*Salix nigra*) and elephant ear (*Colocasia esculenta*).  
115 Intertidal zones are between mean high and low water level (-0.4 to 0.3 m NAVD88) and  
116 experience regular flood-drain cycles, while subtidal zones (<-0.4 m NAVD88) are persistently  
117 inundated year-round. The water level in these zones is primarily influenced by river stage, wind,  
118 and storms and partly driven by (semi-)diurnal tides (<0.3 m total water level change).<sup>12,34</sup>  
119 Emergent forbs (e.g., *Sagittaria* spp) and American lotus (*Nelumbo lutea*) are common in  
120 periodically-inundated intertidal zones, while emergent macrophytes dominate the subtidal zones  
121 (e.g., *Eichhornia* spp., *Nymphaea* spp.).  
122

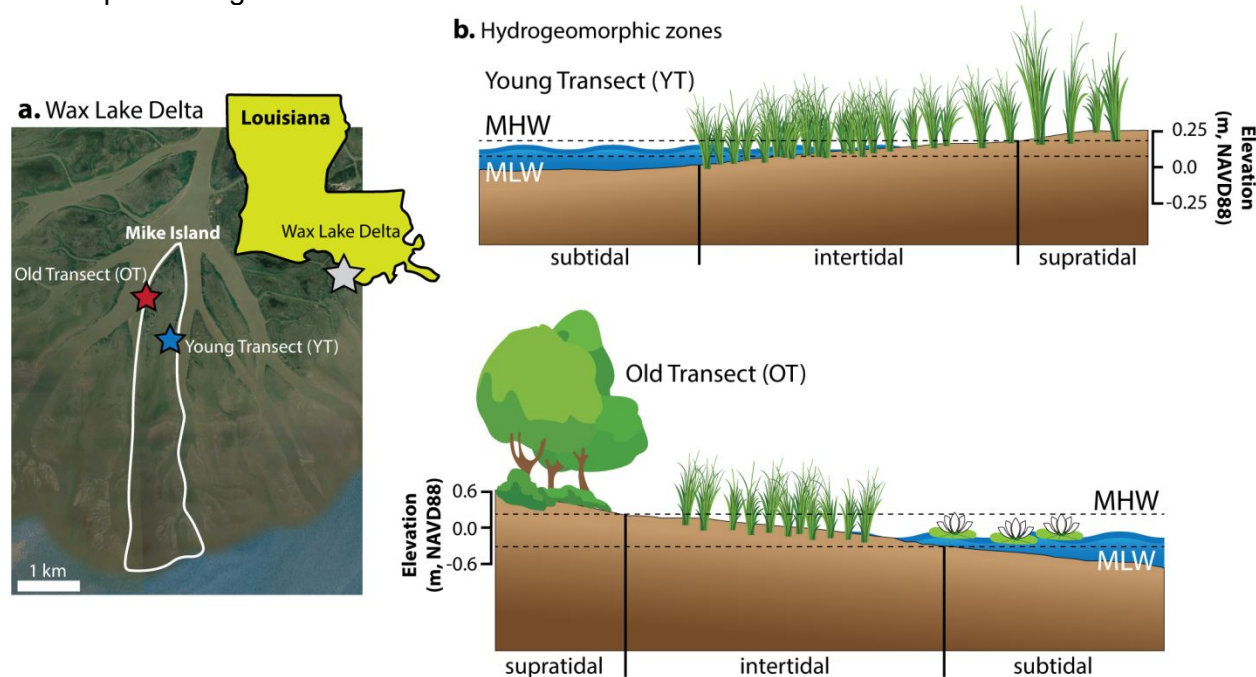
123 Soils in the WLD also display clear vertical and lateral differentiation across hydrogeomorphic  
124 zones.<sup>17,35,36</sup> The sediment being transported to and deposited within the WLD is dominated by  
125 coarse silt to very fine sand materials.<sup>37,38</sup> Frequent inundation and sediment resuspension in  
126 subtidal zones maintains mineral-rich, fine-grained soils with high water content, low bulk density  
127 (mean 0.24 g·cm<sup>-3</sup>), and minimal organic carbon (<0.02 g·cm<sup>-3</sup>). Intertidal zones that experience  
128 periodic inundation support dense vegetation that traps sediment and contributes organic matter,  
129 resulting in more consolidated soils (mean bulk density 0.68 g·cm<sup>-3</sup>), with slightly elevated organic  
130 carbon (~0.01 g·cm<sup>-3</sup>) and shallow redox gradients. In supratidal zones, soils are infrequently  
131 flooded, more oxidized, and increasingly organic-rich (~0.02 g·cm<sup>-3</sup>), showing early pedogenic  
132 features and greater root biomass.  
133

### 134 **Soil collection**

Open Access Article. Published on 06 May 2022. Downloaded on 5/7/2022 6:46:05 PM.  
This article is licensed under a Creative Commons Attribution-NonCommercial 3.0 Unported Licence.  
CC BY-NC

1  
2  
3 135 Surface soils were collected from two elevation transects on Mike Island in the WLD that exhibit  
4 136 differences in time since subaerial emergence, soil properties, and vegetation types (Figure 1b).  
5 137 The “Old Transect” (OT; 29.51009, -91.44449) is in the proximal sedimentation region of Mike  
6 138 Island and first became subaerial between 1987–1995, whereas the “Young Transect” (YT;  
7 139 29.49438, -91.44121) is closer to the active delta front and became subaerial between 2001–  
8 140 2005 (Figure S1).<sup>11</sup> The OT exhibits pronounced ecological succession along the island’s  
9 141 elevation gradient, transitioning from forested wetlands (primarily *Salix nigra*) in supratidal zones  
10 142 to marsh dominated species in intertidal (e.g., *Sagittaria* spp., *Colocasia* spp.) and subtidal  
11 143 regions.<sup>39–41</sup> The YT includes primarily intertidal and subtidal hydrogeomorphology with vegetation  
12 144 mainly consisting of sawgrass and submerged and floating-leafed (*Potamogeton nodosus*)  
13 145 vegetation.<sup>42,43</sup> In the text, we use “Old Transect” and “Young Transect” strictly to reference the  
14 146 island age (i.e., time since subaerial emergence) rather than features of soil development and/or  
15 147 weathering.  
16 148

17 149 Triplicate shallow soil cores (0–30 cm depth) were collected in March 2023 from within a 1 m x 1  
18 150 m plot at each sampling location by manually inserting a 5 cm diameter acrylic soil core liner  
19 151 (AMS, Inc.) into the soil until the 30 cm core liner was flush with the ground surface. The core  
20 152 liners were immediately capped and sealed in gas impermeable bags containing an oxygen-  
21 153 scrubbing pouch (AnaeroPack™, Mitsubishi Chemical Corp.) to preserve anoxic conditions. Soils  
22 154 experienced compaction during sampling that resulted in each core liner containing headspace  
23 155 derived from the subsurface environment. The samples were held on ice and frozen within 6 h of  
24 156 collection, then shipped overnight to Oak Ridge National Laboratory and stored at -20 °C until  
25 157 further processing.

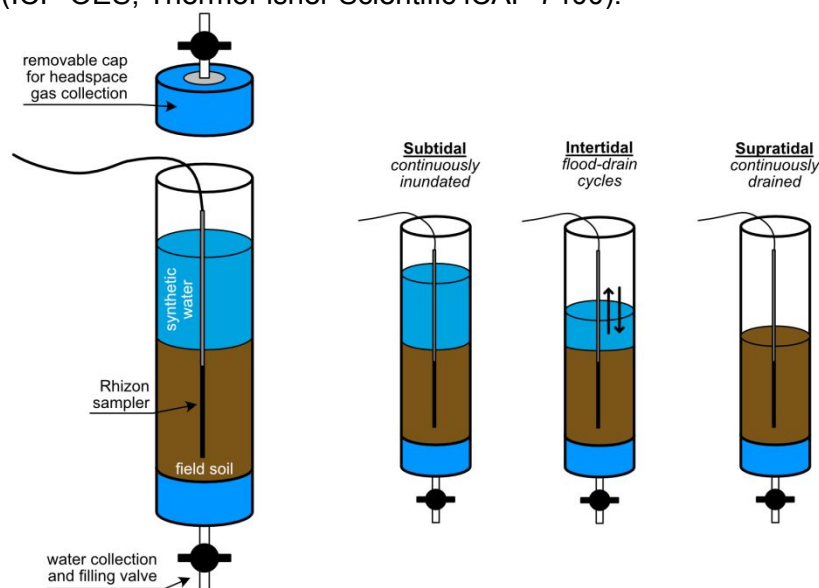


158  
159 **Figure 1.** (a) Map of Old Transect (OT) and Young Transect (YT) study sites on Mike Island in  
160 the Wax Lake Delta, Louisiana. (b) Conceptual illustration of hydrogeomorphic zones at Old  
161 Transect (OT) and Young Transect (YT) study areas. Approximate ground surface elevations and  
162 ecological zones are derived from Twilley et al. (2019).<sup>10</sup>  
163

### 164 **Mesocosm setup and initial soil characterization**

165 Incubation mesocosms were constructed from the acrylic core liners used for soil collection  
 166 (diameter 5 cm, height 30 cm; Figure 2). The frozen soils were placed in an anaerobic chamber  
 167 (97.5% N<sub>2</sub>:2.5% H<sub>2</sub>; Coy, Inc.) and allowed to thaw completely at room temperature (~12 h). The  
 168 thawed soils were removed from the liners, transferred into a 1 L acid-washed glass crystallization  
 169 dish, and manually homogenized with an acid-washed glass rod and subsampled for pH (1:1 in  
 170 0.01 M CaCl<sub>2</sub>), total C and N (Elementar UNICUBE®), and selective chemical extractions. After  
 171 subsampling soils for initial characterization, they were then transferred back into the core liners,  
 172 and the bottom cap was replaced with a cap containing a two-way valve to allow controlled  
 173 drainage of the mesocosm. A layer of polyester filter cloth (5 μm pore size) was placed inside the  
 174 cap to prevent the loss of soil while draining and filling the mesocosms. Due to limited quantities  
 175 of soil from the OT intertidal zone, the triplicate soil samples were combined, homogenized, and  
 176 split into duplicate mesocosms; all other incubations were performed in triplicate.

178 Selective chemical extractions were performed inside the anaerobic chamber to quantify  
 179 concentrations of Fe and P associated with different solid Fe mineral phases. Subsamples for the  
 180 extractions were dried under N<sub>2</sub> atmosphere in the glove box. The iron extractions followed  
 181 previously described methods.<sup>44,27,45</sup> Briefly, short-range ordered (SRO) Fe(III) oxyhydroxides  
 182 (e.g., ferrihydrite, lepidocrocite) were extracted for 48 h with 1 M Hydroxylamine-HCl in 25% (v/v)  
 183 acetic acid. Total redox-sensitive Fe(III) (oxyhydr)oxides were extracted for 2 h with freshly  
 184 prepared citrate-buffered sodium dithionite (50 g·L<sup>-1</sup> sodium dithionite in 0.35 M acetic acid and  
 185 0.2 M sodium citrate buffer, pH 4.8). Long-range ordered (LRO) Fe(III) oxide minerals (e.g.,  
 186 crystalline goethite, hematite) were calculated as the difference between total-redox sensitive  
 187 Fe(III) (oxyhydr)oxides and SRO Fe(III) oxyhydroxides. Each extraction protocol was performed  
 188 by placing ~1.0 g of dried soil and 10 mL of the extractant solution in a 50 mL conical tube on an  
 189 end-over-end rotator. The resulting soil slurries were centrifuged (30 min at 4000 rcf), and the  
 190 supernatants were filtered (<0.45 μm nylon syringe filter) and acidified with 2-3 drops of trace  
 191 metal grade nitric acid for analysis by inductively coupled plasma-optical emission spectroscopy  
 192 (ICP-OES; ThermoFisher Scientific iCAP 7400).



193  
 194 **Figure 2.** Schematic of mesocosms used for laboratory soil incubations. **(Left)** Example  
 195 mesocosm containing field-collected soil and synthetic water. The valve at the bottom was used  
 196 to fill and drain the mesocosms while the Rhizon sampler was used to collect in-situ porewater.  
 197 The removable cap was periodically attached to the top of each mesocosm for headspace gas



198 collection. **(Right)** Illustration of the three different incubation conditions. All mesocosms were  
199 constructed identically regardless of reaction conditions.

### 201 **Mesocosm incubation and sampling**

202 The constructed mesocosms were transferred to the benchtop and incubated for 30 days at room  
203 temperature (20–22°C) to match the mean annual temperature of the Wax Lake Delta (20.3°C).  
204 To reflect field inundation conditions, supratidal mesocosms were incubated without additional  
205 water for 21 days, at which point the soils were rewetted to approximately field capacity due to  
206 visible drying of the soils. Because soil moisture was not measured in the field, field capacity was  
207 visually estimated by adding water until soils appeared moist throughout but not saturated.  
208 Subtidal mesocosms were continuously inundated at 15 cm above the soil surface to reflect the  
209 average water depth of the subtidal zone on Mike Island.<sup>34</sup> Intertidal mesocosms underwent four  
210 flood-drain cycles over the 30-day experiment. The composition of the solution used to inundate  
211 the intertidal soils reflected the concentrations of major ions measured in surface water at the field  
212 site during soil collection (100  $\mu\text{mol}\cdot\text{L}^{-1}$  sulfate from  $\text{Na}_2\text{SO}_4$ , 420  $\mu\text{mol}\cdot\text{L}^{-1}$  chloride from  $\text{NaCl}$ ; see  
213 additional details in Table S1). The solution was prepared in deionized water and did not contain  
214 any solutes other than sodium, chloride, and sulfate. The first porewater measurement during the  
215 incubations captured the initial concentrations of solutes derived from the soil. The solution pH  
216 was 7.5, as prepared, and was not adjusted before use. During the flood-drain cycles, water from  
217 the intertidal mesocosms was gravity drained from the port on the bottom end cap. After the water  
218 was allowed to self-drain, any water that remained pooled on the soil surface was carefully  
219 removed by using a syringe connected to the port on the bottom cap to apply vacuum. For  
220 subsequent inundated periods, the water level was returned to 15 cm above the soil surface by  
221 slowly injecting fresh synthetic water upwards through the port on the bottom of the mesocosms,  
222 taking care to avoid disturbing the soil.

224 Before beginning the incubations, one Rhizon porewater sampler (0.15  $\mu\text{m}$  pore size, 10 cm  
225 membrane length; Rhizosphere Research Products) was installed vertically into the center of the  
226 soil and left in place throughout the duration of the experiment. The rhizon spanned the top 10  
227 cm of the mesocosm soil. The top of each mesocosm was loosely covered with semi-transparent  
228 plastic film to prevent evaporation and drying. Porewater from subtidal and intertidal mesocosms  
229 was collected through an acid-washed syringe (10% HCl) attached to the Rhizon sampler and  
230 subsequently analyzed for concentrations of dissolved organic C (DOC), P, Ca, Mg, total Fe, and  
231  $\text{Fe}^{2+}$ , pH, specific conductance, and oxidation-reduction potential (ORP; mV vs Ag/AgCl).  
232 Porewater was not collected from supratidal mesocosms due to insufficient volume available for  
233 chemical analyses. Dissolved organic carbon was measured with a total organic carbon analyzer  
234 (Shimadzu TOC-L). Total dissolved elements were quantified by ICP-OES. Concentrations of  $\text{Fe}^{2+}$   
235 were quantified by the 1,10-phenanthroline assay in a UV-Vis spectrophotometer.<sup>46</sup> Specific  
236 conductance, pH, and ORP were measured with a handheld multiparameter probe. ORP values  
237 were converted (+209 mV) to redox potentials relative to the standard hydrogen electrode ( $E_h$ ).

239 To maintain a consistent water volume in each mesocosm, the volume of water removed during  
240 each sampling (~20 mL) was immediately replaced with fresh solution. At the end of the  
241 experiment, the mesocosms were transferred back into the anaerobic chamber, the soils were  
242 removed from the liners and homogenized, then analyzed for total C and N concentrations and  
243 hydroxylamine and dithionite-extractable Fe and P.

### 245 **Carbon dioxide flux measurements**

246 Carbon dioxide ( $\text{CO}_2$ ) fluxes (as  $\text{mmol CO}_2\text{-C m}^{-2}\cdot\text{d}^{-1}$ ) were determined by sealing the mesocosms  
247 with a cap fitted with a butyl rubber septum (Figure 2) and collecting a 15 mL aliquot of headspace

248 gas three times over a 24 h period. The CO<sub>2</sub> concentrations were measured by gas  
249 chromatography (GC; Shimadzu Corp.). Flux values were calculated according to eqn 1:

$$250 \text{ soil CO}_2 \text{ flux} = \frac{\partial c}{\partial t} * \frac{V}{A_s} (1)$$

251 where c is the concentration of CO<sub>2</sub> in the headspace (in ppm<sub>v</sub>), V is the headspace volume of  
252 each mesocosm (in m<sup>3</sup>), A<sub>s</sub> is the soil surface area (19.6 cm<sup>2</sup>), and t is the total collection time (in  
253 hr). A linear regression of the three concentration measurements made during each 24 h  
254 collection period ( $\partial C/\partial t$ ) was applied to determine the CO<sub>2</sub> flux. To account for the differences in  
255 soil C concentration across sites, CO<sub>2</sub> fluxes were normalized to the total C concentration in the  
256 initial bulk soils (in mol CO<sub>2</sub>-C·mol C<sup>-1</sup>). Methane (CH<sub>4</sub>) and nitrous oxide (N<sub>2</sub>O) were also  
257 measured and were below the detection limit in all samples.

### 259 **Data and Statistical Analysis**

260 All data analyses were performed using in R (v4.3.0).<sup>47</sup> We used *dplyr* (v1.1.4) for data wrangling  
261 and processing; *ggplot2* (v3.5.2)<sup>48</sup> and *cowplot* (v1.2.0) for data visualization; and *stats* (v4.5.2)  
262 and *vegan* (v2.7-2) for multivariate statistics. We used PERMANOVA (Bray-Curtis; permutations:  
263 999) to evaluate overall trends across transect location (OT vs. YT) and transect position  
264 (supratidal vs. intertidal vs. subtidal). Linear mixed-effects models (LME) and ANOVA were used  
265 to determine trends of individual analytes and compare means. Statistical significance was  
266 determined at  $\alpha = 0.05$ . Values of F and p reported in the text are from PERMANOVA analyses,  
267 unless otherwise stated. All analytical results with uncertainties are reported as the mean  $\pm$   
268 standard deviation.

270 Cumulative solute releases for subtidal mesocosms were calculated incrementally by multiplying  
271 the solute concentration at each sampling point by the total mesocosm liquid volume. For intertidal  
272 mesocosms which were periodically drained, cumulative releases were determined as solute  
273 concentration times liquid volume at each time of draining summed over all drainages. We  
274 assumed that solute concentrations reached equilibrium between sampling points and did not  
275 adjust values for potential dilution due to replenishing water volume removed through sampling in  
276 each mesocosm.

## 278 **Results and Discussion**

### 279 **Soil characteristics influenced by delta age and inundation patterns**

280 Overall, transect position (supratidal vs. intertidal vs. subtidal) accounted for 51% of total variation  
281 in soil biogeochemical analytes (F = 53, p < 0.001), whereas transect location (OT vs. YT)  
282 accounted for 4% (F = 8, p = 0.0097). Within transects, soil C, N, and pH decreased in the order  
283 intertidal > supratidal > subtidal; the sole exception was soil pH in YT, where subtidal values were  
284 higher than in supratidal (Table 1). Total Fe oxides (SRO oxyhydroxides and LRO oxides) were  
285 high in the supratidal zones, particularly at the OT, and decreased with decreasing elevation.  
286 These values align with previously reported data from Mike Island (15–36 g·kg<sup>-1</sup> C; 1.2–2.6 g·kg<sup>-1</sup>  
287 N; 30–180  $\mu\text{mol}\cdot\text{g}^{-1}$  Fe) and reflect higher overall concentrations of C, N, and Fe and lower pH in  
288 older delta regions.<sup>17,49</sup>

290 Short-range ordered and crystalline Fe oxides varied in abundance across both transects.  
291 Intertidal and subtidal soils contained primarily SRO Fe oxides, whereas supratidal soils had  
292 similar proportions of SRO and LRO Fe (~1:1 molar ratio). Higher relative proportions of SRO Fe  
293 oxides in intertidal and subtidal zones may (i) indicate rapid re-formation of metastable phases,  
294 offsetting transformation of SRO Fe to more crystalline LRO phases under successive redox  
295 cycles or (ii) retention of metastable phases under persistently anoxic subtidal conditions where  
296 transformation to crystalline oxides is kinetically limited.<sup>28,50,51</sup> This observation is consistent with

297 previous findings that coastal wetlands are preferentially enriched in SRO Fe minerals relative to  
298 upland soils.<sup>50</sup> As deltaic islands gain elevation, soils transition from primarily anoxic conditions  
299 (subtidal) to variable anoxic-oxic cycles (intertidal) then primarily oxic conditions (supratidal),<sup>11</sup>  
300 thus, providing important evidence that differences in Fe abundance and mineral form across the  
301 transects illustrate that Fe redox cycling may play important and evolving roles in biogeochemical  
302 processes during delta formation.

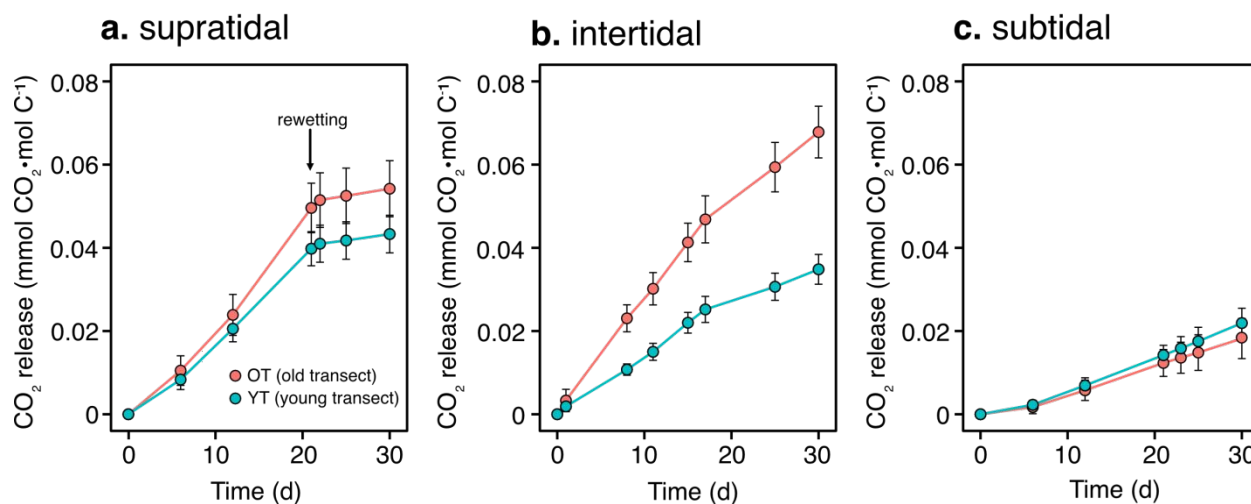
303  
304 **Table 1.** Chemical properties of the bulk soil used for the incubation experiments. Concentrations  
305 of short-range ordered (SRO) and long-range ordered (LRO) Fe oxides were determined from  
306 selective chemical extractions. All values represent the mean  $\pm$  standard deviation (n=3). Letters  
307 represent significant differences within each column (Tukey HSD,  $\alpha = 0.05$ ).

Transect	Tidal zone	Soil pH (-)	C (g·kg <sup>-1</sup> )	N (g·kg <sup>-1</sup> )	SRO Fe ( $\mu\text{mol Fe}\cdot\text{g}^{-1}$ )	LRO Fe* ( $\mu\text{mol Fe}\cdot\text{g}^{-1}$ )	SRO/LRO (-)
Old	Supratidal	7.17 $\pm$ 0.01 <sup>C</sup>	37.6 $\pm$ 1.1 <sup>B</sup>	4.2 $\pm$ 0.3 <sup>A</sup>	139 $\pm$ 4 <sup>C</sup>	144 $\pm$ 8 <sup>A</sup>	1.0 $\pm$ 0.1
	Intertidal	7.18 $\pm$ 0.09 <sup>BC</sup>	48.6 $\pm$ 1.9 <sup>A</sup>	5.1 $\pm$ 0.1 <sup>A</sup>	101 $\pm$ 1 <sup>A</sup>	4 $\pm$ 5 <sup>C</sup>	3.0 $\pm$ 2.4
	Subtidal	7.16 $\pm$ 0.08 <sup>C</sup>	29.2 $\pm$ 1.1 <sup>C</sup>	1.7 $\pm$ 0.3 <sup>B</sup>	69 $\pm$ 1 <sup>B</sup>	13 $\pm$ 2 <sup>C</sup>	5.4 $\pm$ 1.1
Young	Supratidal	7.41 $\pm$ 0.13 <sup>AC</sup>	19.7 $\pm$ 0.7 <sup>D</sup>	1.3 $\pm$ 0.4 <sup>B</sup>	96 $\pm$ 1 <sup>A</sup>	85 $\pm$ 1 <sup>B</sup>	1.1 $\pm$ 0.1
	Intertidal	7.51 $\pm$ 0.15 <sup>A</sup>	20.4 $\pm$ 2.8 <sup>D</sup>	1.7 $\pm$ 0.2 <sup>B</sup>	85 $\pm$ 1 <sup>D</sup>	7 $\pm$ 1 <sup>C</sup>	4.7 $\pm$ 3.1
	Subtidal	7.49 $\pm$ 0.02 <sup>AB</sup>	18.1 $\pm$ 1.4 <sup>D</sup>	1.2 $\pm$ 0.3 <sup>B</sup>	59 $\pm$ 1 <sup>E</sup>	1 $\pm$ 2 <sup>C</sup>	5.4 $\pm$ 1.0

\*Calculated as the difference between dithionite- and hydroxylamine-extractable Fe.

### 308 **CO<sub>2</sub> production enhanced by variable inundation**

309 We investigated CO<sub>2</sub> production throughout the experiment to determine how inundation patterns  
310 affected organic matter decomposition, and whether these observations were consistent across  
311 space (OT vs. YT) and time (Figure 3). Similar to soil properties, transect position accounted for  
312 significantly more of the total variation in both cumulative CO<sub>2</sub> release and average CO<sub>2</sub> flux (F =  
313 27.6, p < 0.001) than transect location (F = 4.8, p = 0.034). In both OT and YT soils, supratidal  
314 and intertidal positions exhibited higher CO<sub>2</sub> production than subtidal soils (Figure 4). Initial rates  
315 of CO<sub>2</sub> release were similar among OT and YT supratidal and OT intertidal soils and higher than  
316 YT intertidal soils. All observed trends in CO<sub>2</sub> flux were consistent whether fluxes were normalized  
317 on a molar (i.e., mmol CO<sub>2</sub>·mol C<sup>-1</sup>·d<sup>-1</sup>), soil dry mass (mmol CO<sub>2</sub>·kg<sup>-1</sup>·d<sup>-1</sup>), or surface area basis  
318 (mmol CO<sub>2</sub>·m<sup>-2</sup>·d<sup>-1</sup>) (Table S1), indicating that differences in flux could be attributed to  
319 biogeochemical processes controlling organic matter decomposition rather than the quantity of  
320 organic matter.



323

 1  
2  
3  
4  
5  
6  
7  
8  
9  
10  
11  
12  
13  
14  
15  
16  
17  
18  
19  
20  
21  
22  
23  
24  
25  
26  
27  
28  
29  
30  
31  
32  
33  
34  
35  
36  
37  
38  
39  
40  
41  
42  
43  
44  
45  
46  
47  
48  
49  
50  
51  
52  
53  
54  
55  
56  
57  
58  
59  
60

**Figure 3.** Cumulative carbon dioxide (CO<sub>2</sub>) release normalized to total soil C during (a) supratidal, (b) intertidal, and (c) subtidal incubations. Error bars represent standard deviation of the mean for triplicate mesocosms. The arrow in panel a indicates when supratidal soils were rewetted. The legend in panel a also applies to panels b–c.

Given the notable shift in CO<sub>2</sub> production after supratidal soils were rewetted (Figure 3a), we analyzed all CO<sub>2</sub> fluxes separately for the time periods before (0–21 d) and after (22–30 d) supratidal rewetting to differentiate the relative effects of soil moisture and incubation time on CO<sub>2</sub> production (Figure 4). Across both transects, average CO<sub>2</sub> fluxes from supratidal and intertidal soils were substantially lower during the second part of the incubation, with a decrease of approximately 85% in supratidal soils and 43% in intertidal soils. Meanwhile, subtidal CO<sub>2</sub> fluxes did not significantly change (Tukey HSD,  $p > 0.05$ ). Although decreases in respiration in the supratidal zones may be an artifact of rewetting, decreasing CO<sub>2</sub> fluxes in intertidal soils could result from decreases in carbon substrates over time. Microbial respiration in a closed system depletes bioavailable substrates, restricting further rates of organic matter decomposition.<sup>52</sup> However, the stable CO<sub>2</sub> fluxes for both subtidal incubations suggests that organic substrates did not become depleted under relatively low respiration rates. Persistent inundation may constrain rates of organic matter decomposition at the lowest elevation regardless of soil properties.

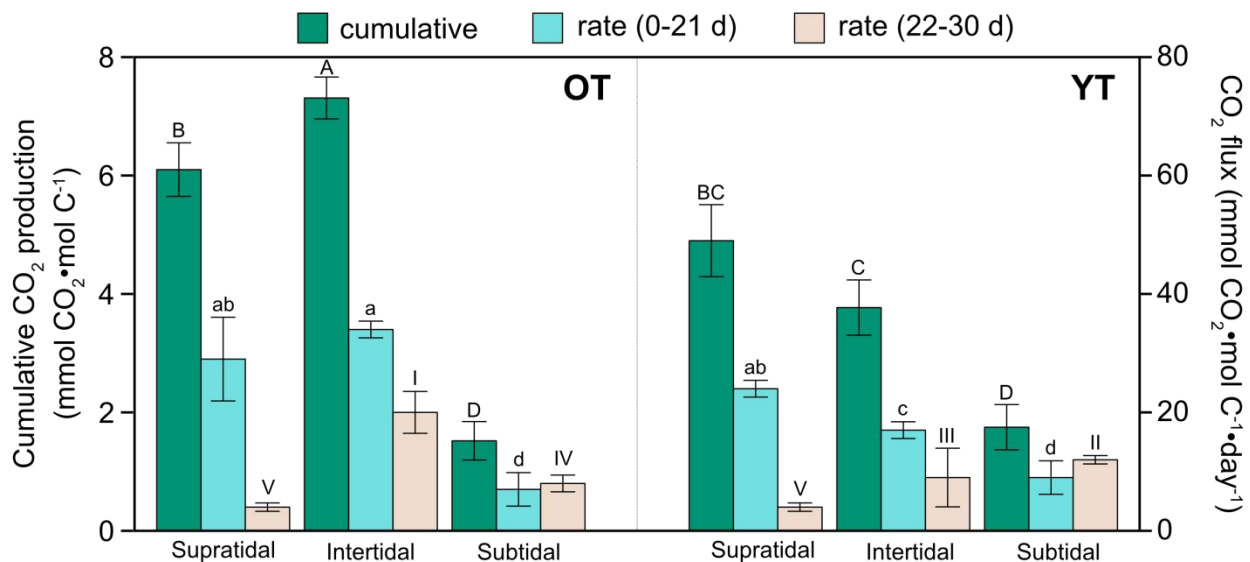


**Figure 4.** CO<sub>2</sub> production across laboratory incubations. Cumulative CO<sub>2</sub> production is shown on the left vertical axis, and average fluxes are shown on the right vertical axis. Fluxes are grouped into days 0-21 and 22-30, corresponding to rewetting of supratidal soils. Bars labeled with different letters are statistically different (Tukey HSD,  $\alpha = 0.05$ ).

#### **Solute mobilization across inundation gradients**

Inundation patterns (i.e., transect position) explained the majority of observed variability in porewater chemistry ( $F = 6.5$ ,  $p = 0.006$ ), with subtidal soils showing significantly lower cumulative releases of most solutes (DOC, Fe, P) than intertidal soils across both transects (Tukey HSD,  $p > 0.05$ ). This pattern was consistent with CO<sub>2</sub> production ( $F = 27.6$ ,  $p < 0.001$ ; Figure 4), indicating that prolonged inundation may reduce overall biogeochemical activity relative to drained or variably inundated conditions. In contrast, solute releases from intertidal soils varied with delta region, with higher releases of DOC, Fe, and P from intertidal soils for OT than YT, while Ca and Mg showed not significant differences between transects (Table S3).

Soil inundation was associated with distinct temporal patterns of solute concentrations that differed between intertidal and subtidal zones (Figure 5). For subtidal soils, most analytes (Fe, P, Ca, pH) increased over time throughout the 30-day incubation, whereas DOC exhibited a sharp initial increase followed by a linear decrease (regression analysis; OT:  $F = 21.98$ ,  $p > 0.001$ ; YT:  $F = 82.27$ ,  $p > 0.001$ ) (Table S3).  $E_h$  remained relatively stable between +54 and +89 mV and cumulative solute releases were greater for OT than YT ( $p > 0.05$ ). For intertidal soils, solute concentrations generally decreased over time but exhibited short pulses of solute release immediately following inundation. Porewater pH gradually increased while  $E_h$  values remained between +45 and +73 mV. Similar to subtidal soils, cumulative solute release from intertidal soils was higher for OT than YT ( $p > 0.05$ ).

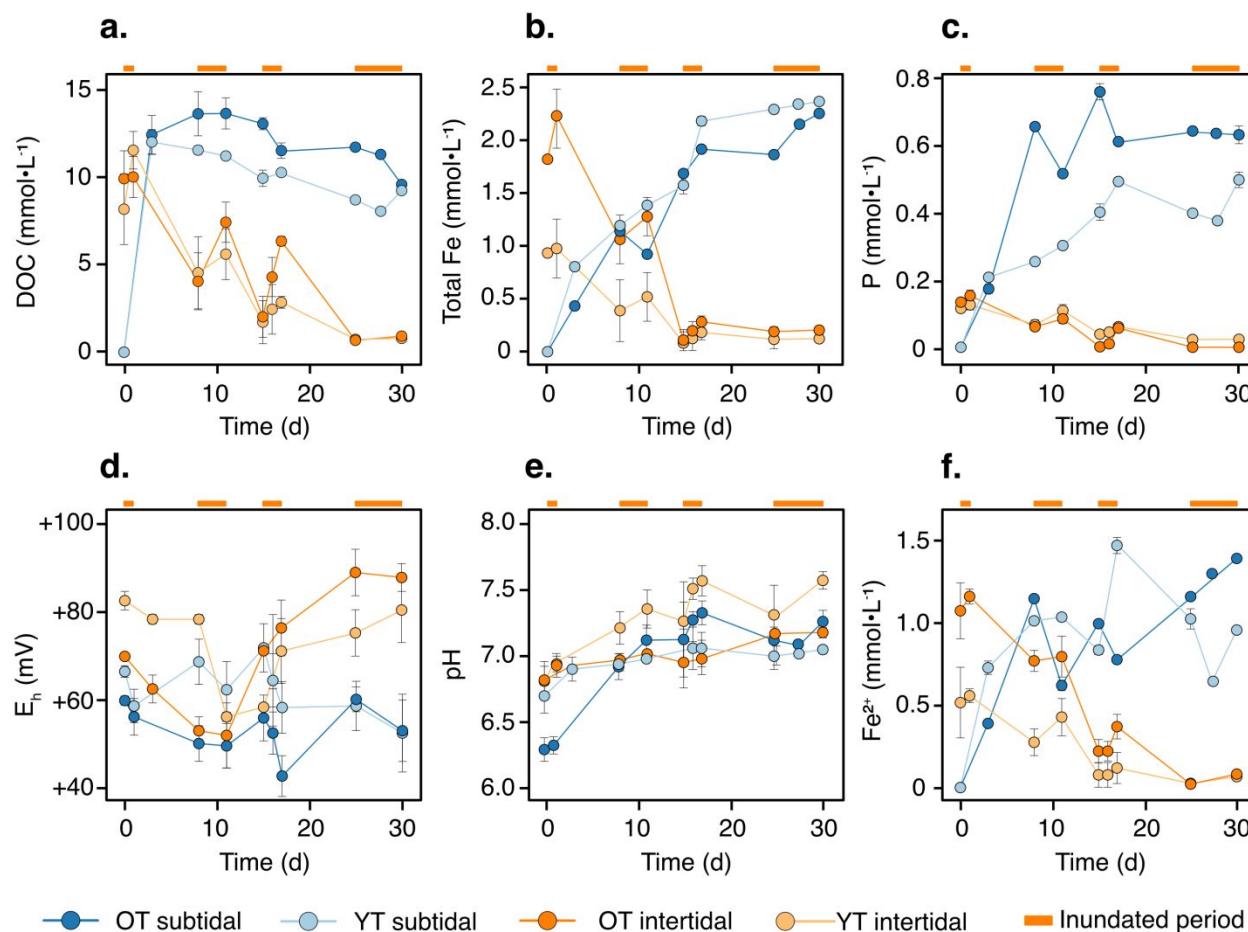


**Figure 5.** Porewater measurements of (a) dissolved organic carbon (DOC;  $\text{mmol}\cdot\text{L}^{-1}$ ), (b) total dissolved iron (Fe;  $\text{mmol}\cdot\text{L}^{-1}$ ), and (c) dissolved phosphorus (P;  $\text{mmol}\cdot\text{L}^{-1}$ ), (d) redox potential ( $E_h$ ; mV vs SHE), (e) pH, and (f) dissolved  $Fe^{2+}$  ( $\text{mmol}\cdot\text{L}^{-1}$ ) during intertidal and subtidal incubations. Error bars represent standard deviations of triplicate mesocosms. The orange bars along the top axis represent inundated periods of intertidal incubations.

Cumulative releases of  $CO_2$  and DOC, expressed as a fraction of total soil C, were compared in order to evaluate the potential for soils to lose C via  $CO_2$  release or DOC leaching. Across all experiments, DOC loss outpaced  $CO_2$  production by a factor of 10 to 67 (Table 3), reflecting the mobility of water-soluble organic matter under inundated conditions. In contrast to individual patterns of  $CO_2$  (Figure 4) and DOC (Figure 5a), transect location (OT vs. YT) had a stronger



effect on DOC:CO<sub>2</sub> ratios ( $F = 28.5$ ,  $p = 0.004$ ) than transect position ( $F = 4.4$ ,  $p = 0.03$ ). Within transects, intertidal DOC:CO<sub>2</sub> values were higher than subtidal for YT (Tukey HSD,  $p < 0.001$ ), while OT showed no significant difference between transect positions (Tukey HSD,  $p = 0.618$ ). These differences in C loss pathways may reflect varying stages of ecosystem development and the balance between C accumulation and decomposition in emerging coastal deltas, as discussed below.

**Table 3.** Fractional loss of C during soil incubations. Values are shown as cumulative losses of C leached (DOC) or respired (CO<sub>2</sub>) divided by the initial amount of C in the bulk soils. DOC:CO<sub>2</sub> are expressed on a molar basis. Values labeled with different letters are statistically different (Tukey HSD,  $\alpha = 0.05$ ).

Transect	Position	DOC Loss (%)	CO <sub>2</sub> Loss (%)	DOC:CO <sub>2</sub>
OT	Supratidal	–	0.02 ± 0.01 <sup>B</sup>	–
	Intertidal	2.30 ± 0.61 <sup>A</sup>	0.14 ± 0.02 <sup>A</sup>	16.4 ± 0.1 <sup>B</sup>
	Subtidal	0.94 ± 0.02 <sup>B</sup>	0.05 ± 0.04 <sup>B</sup>	18.8 ± 7.7 <sup>B</sup>
YT	Supratidal	–	0.01 ± 0.01 <sup>B</sup>	–
	Intertidal	2.52 ± 0.22 <sup>A</sup>	0.04 ± 0.02 <sup>B</sup>	63.0 ± 4.2 <sup>A</sup>
	Subtidal	1.08 ± 0.01 <sup>B</sup>	0.05 ± 0.03 <sup>B</sup>	21.6 ± 2.8 <sup>B</sup>

### Processes regulating biogeochemical activity

The patterns of reduced biogeochemical activity in subtidal zones and enhanced activity in intertidal and supratidal zones are consistent with established conceptual models linking enhanced carbon cycling to environments that experience periodic redox fluctuations rather than persistently oxic or anoxic conditions.<sup>53–57</sup> In WLD, supratidal and intertidal soils are subject to redox shifts driven by episodic flooding and tidal exchange, respectively, whereas subtidal soils remain primarily inundated and anoxic.<sup>58</sup> Redox transitions in intermittently flooded soils can stimulate microbial metabolisms by increasing the availability of electron acceptors,<sup>59,60</sup> promoting organic matter turnover,<sup>61–63</sup> and regenerating reactive mineral phases,<sup>64,65</sup> thereby driving both CO<sub>2</sub> production and solute mobilization.<sup>59</sup> Thus, delta regions representing later stages of island development (i.e., higher elevation relative to water level) are likely to support higher rates of biogeochemical activity than younger, predominantly subtidal areas. This linkage between elevation, inundation regime, and metabolic activity highlights the importance of geomorphic evolution in regulating carbon and nutrient cycling in active freshwater deltas.<sup>10</sup>

Successional development in WLD is further accompanied by systematic changes in soil chemistry and physical structure (Table 1).<sup>10,66</sup> Younger, frequently inundated soils are dominated by dense, mineral-rich riverine sediments, characterized by low organic C (1.7–2.4%) and N (0.08–0.18%) concentrations, and high C:N ratios. In contrast, as island elevation increases and inundation frequency decreases, soils transition toward more organic inputs from emergent vegetation, resulting in higher C (2.8–5.1%) and N (0.14–0.52%) concentrations with lower C:N ratios.<sup>11,49,66</sup> Reduced hydroperiods in supratidal and intertidal zones promote episodic oxygen exposure, enhance root penetration, and facilitate the development of more structurally complex and biogeochemically active soils.<sup>67–69</sup> These transitions in soil composition and structure likely amplify redox variability and substrate availability,<sup>70</sup> reinforcing higher rates of CO<sub>2</sub> production and solute mobilization in intertidal and supratidal soils. Collectively, our results indicate that inundation regime may exert an important control on carbon cycling during deltaic evolution.

### Phosphorus retention modified by Fe redox cycling

423 The strong positive correlations between cumulative  $\text{Fe}^{2+}$  and P release (Figure 6a and d;  
424 regression analysis,  $p < 0.05$ ) suggest a strong influence of Fe oxides on P solubility, although  
425 organic matter or other minerals may also play an important role. Variable inundation across WLD  
426 drives frequent redox oscillations<sup>58</sup> that may promote the formation of SRO Fe oxides<sup>71</sup> with  
427 available surfaces for binding phosphate.<sup>27,72</sup> Further, persistent anoxia (i.e., due to inundation)  
428 has been linked to microbial respiration of Fe oxides, potentially releasing large amounts of  
429 phosphate from WLD soils with comparatively low releases under aerobic (e.g., drained)  
430 conditions.<sup>15</sup> The Fe reducing conditions ( $<100$  mV at pH 7), increasing pH, and fluctuating  $\text{Fe}^{2+}$   
431 concentrations in our study (Figure 5d-f) were all key indicators of Fe redox cycling.<sup>73,74</sup> Thus, we  
432 infer that Fe reductive dissolution was an important source of P to the soil porewater in our study.  
433 Soil Fe oxides may also affect DOC mobility through sorption and co-precipitation interactions  
434 with organic matter;<sup>17,75,76</sup> however,  $\text{Fe}^{2+}$  and DOC correlations (Figure 6c-d) were weaker than for  
435  $\text{Fe}^{2+}$  and P, and linear (regression analysis,  $p < 0.05$ ) only for intertidal soils, indicating that Fe  
436 reductive dissolution had a stronger influence on P retention than on DOC.

437  
438 Organic matter decomposition may have also influenced P mobility in our experiments, with  
439 release of organic-P into porewater providing available substrates for phosphate cleavage by  
440 phosphatase enzymes.<sup>77</sup> Further, P may have interacted with species other than Fe oxides and  
441 organic matter entirely, including Ca, aluminum (Al), and non-oxide Fe. In coastal systems with  
442 high concentrations of Ca, Al, and dissolved  $\text{Fe}^{2+}$ , phosphate can sorb to Al- and Ca-oxides<sup>72,78–80</sup>  
443 or precipitate with metal cations to form compounds including hydroxyapatite ( $\text{Ca}_{10}(\text{PO}_4)_6(\text{OH})_2$ )  
444 and vivianite ( $\text{Fe}^{II}_3(\text{PO}_4)_2 \cdot 8\text{H}_2\text{O}$ ).<sup>81</sup> Although these species can have a strong influence on P  
445 mobility in coastal wetlands, their capacity for P retention is determined primarily by changes in  
446 pH rather than fluctuations in  $E_h$ .<sup>82–84</sup> For example, the optimal pH range for P fixation is ~5–6 for  
447 Al and ~8–9 for Ca,<sup>85</sup> well outside the pH range in our study (6.4–7.7; Figure 5e). In addition, our  
448 linear regression analyses revealed progressively weaker correlations of  $\rho(\text{P}, \text{Fe}) > \rho(\text{P}, \text{DOC}) >$   
449  $\rho(\text{P}, \text{Ca})$ , while Al concentrations were below the instrumental detection limit in all samples (data  
450 not shown). Overall, our results do not rule out the potential role of pH, base cations, and organic  
451 matter in regulating P mobility,<sup>75,77,86</sup> but support that Fe oxide cycling was the strongest contributor  
452 to P release of the measured analytes in our experiment.  
453

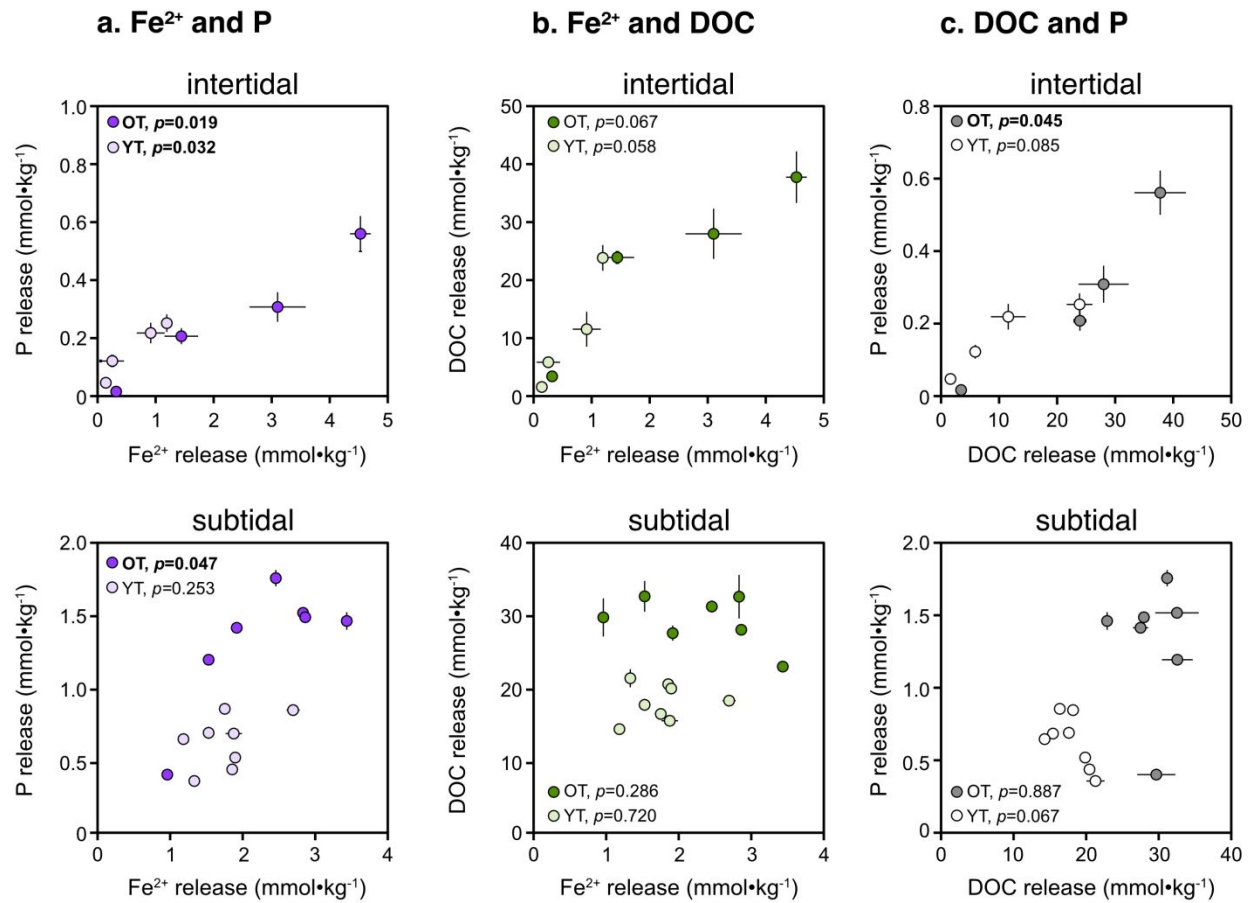


**Figure 6.** Correlations between cumulative Fe<sup>2+</sup> and P, (b) Fe<sup>2+</sup> and DOC, and (c) DOC and P release in intertidal and subtidal incubations. Error bars represent standard deviations of triplicate mesocosms. P values indicate goodness of fit for linear regression analysis ( $\alpha = 0.05$ ). P values for significant linear correlations are shown in bold.

454  
455  
456  
457  
458  
459

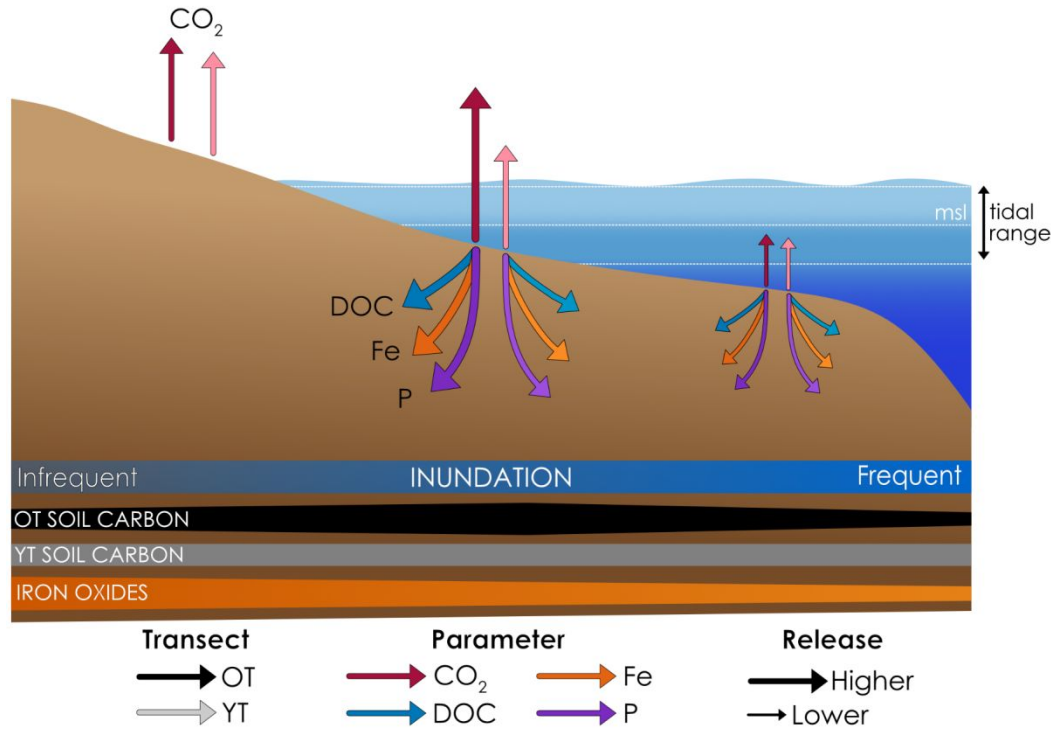


**Figure 7.** Conceptual diagram of solute and carbon dioxide (CO<sub>2</sub>) dynamics under variable inundation of freshwater coastal soils. The shaded blue area represents the tidal range, with more frequently inundated areas shown in darker colors. The white dashed lines represent mean sea level (msl), high tide, and low tide. Arrows represent the release of dissolved organic carbon (DOC), total dissolved iron (Fe) and phosphorus (P), and CO<sub>2</sub>. Horizontal bars at the bottom of the figure indicate relative concentrations of total soil carbon and Fe(III) (oxyhydr)oxides. Note that porewater solutes could not be sampled in the supratidal soils.

### Limitations to experimental approach

Due to logistical constraints, soil samples were frozen prior to analysis rather than analyzed fresh. Freezing can affect microbial activity<sup>87</sup> and Fe mineral characteristics;<sup>88,89</sup> however, all samples were treated identically and frozen for the same duration (~2 weeks), standardizing potential effects. Moreover, freezing has been shown to have minimal impact on overall soil biochemical properties.<sup>87,90,91</sup> We observed no significantly elevated CO<sub>2</sub> fluxes at early timepoints, indicating freezing artifacts did not prominently affect our results. Additionally, any changes to Fe oxide concentrations would have occurred uniformly across treatments, leaving our relative comparisons across inundation conditions unaffected.

We also emphasize that our P measurements by ICP-OES quantify *total P* and cannot differentiate between inorganic P (i.e., phosphate) and P contained in organic matter (i.e., organic P). This is an important distinction because inorganic phosphate is the readily bioavailable form of P while organic-P must be enzymatically cleaved from organic matter prior to microbial uptake.<sup>92,93</sup> As such, our data can reveal potential factors regulating P mobilization in emerging deltaic systems but cannot be used to directly infer bioavailability of the released P.

### Conclusions

Emerging freshwater deltas experience dynamic hydrological regimes that may influence the fate of C and nutrients being exported from inland to open water systems. As deltas emerge, elevation gradients form that affect the frequency of soil inundation and could alter the interactions of OC

1  
2  
3 490 and nutrients in the soil, and the biogeochemical processes that drive their transformation and/or  
4 491 release. This study improves our understanding of the potential influences of soil chemical  
5 492 properties and inundation on C and P release from emerging deltaic systems (Figure 7). Our  
6 493 results suggest that older delta regions may supports higher rates of biogeochemical activity in  
7 494 supratidal and intertidal eco-hydrogeomorphic zones, presumably due to differences in soil  
8 495 chemical properties. Furthermore, inundation-driven redox oscillations in intertidal zones can  
9 496 enhance the decomposition of soil organic matter into carbon dioxide and accelerate the turnover  
10 497 of Fe(III) (oxyhydr)oxide minerals. In subtidal zones, soil saturation may restrict O<sub>2</sub> availability for  
11 498 OM decomposition and inhibit the formation of Fe-OC and Fe-P associations, exerting a stronger  
12 499 control over biogeochemical processes than soil properties. Microbial respiration of Fe oxides  
13 500 may be an important pathway for sustaining OM decomposition and P release under anoxic  
14 501 conditions. These results illustrate the interplay of hydrologic and geomorphic factors in delta  
15 502 soils, emphasizing the importance of emerging ecosystems as biogeochemical hotspots<sup>94,95</sup> –  
16 503 where redox shifts from water level fluctuations cause repeated Fe reductive dissolution under  
17 504 oxic conditions and precipitation of SRO Fe oxyhydroxides under oxic conditions,<sup>71,96</sup> As reactive  
18 505 Fe minerals can be a large part of total soil Fe in WLD and coastal ecosystems more broadly,<sup>17,97</sup>  
19 506 future work should address how Fe(III) phases will change over time, particular regarding their  
20 507 ability to influence carbon burial and buffer high nutrient loads from inland ecosystems.

### 508 **Conflicts of interest**

509 There are no conflicts to declare.

### 510 **Data availability**

511 The raw data supporting this article have been included as part of the Supplementary Information.

### 512 **Acknowledgements**

513 We would like to thank Andre Rovai and Robert Twilley for access to field sites and assistance  
514 with site selection at Wax Lake Delta. In addition, we thank Michale Jones for assisting in the field  
515 collecting soil samples and student interns Kayla Summerlot and Georgie McDevitt for assisting  
516 with incubation experiments and soil processing. This work is supported by grant ERKPA45  
517 through the U.S. Department of Energy, Office of Science, Office of Biological and Environmental  
518 Research, Environmental System Science program under Funding Opportunity DE-FOA-  
519 0002563.

### 520 **References**

- 521  
522  
523  
524  
525 (1) Sawyer, A. H.; Edmonds, D. A.; Knights, D. Surface Water-groundwater Connectivity in  
526 Deltaic Distributary Channel Networks. *Geophys. Res. Lett.* **2015**, *42*, 10299–10306.  
527 <https://doi.org/10.1002/%202015GL066156>.  
528 (2) Savoie, A. M.; Moody, A.; Gilbert, M.; Dillon, K. S.; Howden, S. D.; Shiller, A. M.; Hayes, C.  
529 T. Impact of Local Rivers on Coastal Acidification. *Limnol. Oceanogr.* **2022**, *67* (12), 2779–  
530 2795. <https://doi.org/10.1002/lno.12237>.  
531 (3) Kirwan, M. L.; Gedan, K. B. Sea-Level Driven Land Conversion and the Formation of Ghost  
532 Forests. *Nat. Clim. Change* **2019**, *9* (6), 450–457. [https://doi.org/10.1038/s41558-019-0488-](https://doi.org/10.1038/s41558-019-0488-7)  
533 *7*.  
534 (4) Bianchi, T. S.; Butman, D.; Raymond, P. A.; Ward, N. D.; Kates, R. J. S.; Flessa, K. W.;  
535 Zamora, H.; Arellano, A. R.; Ramirez, J.; Rodriguez, E. The Experimental Flow to the  
536 Colorado River Delta: Effects on Carbon Mobilization in a Dry Watercourse. *J. Geophys. Res.*  
537 *Biogeosciences* **2017**, *122* (3), 607–627. <https://doi.org/10.1002/2016JG003555>.  
538 (5) Richter, B. D.; Baumgartner, J. V.; Powell, J.; Braun, D. P. A Method for Assessing Hydrologic  
539 Alteration within Ecosystems. *Conserv. Biol.* **1996**, *10* (4), 1163–1174.  
540 <https://doi.org/10.1046/j.1523-1739.1996.10041163.x>.



- 1  
2  
3 541 (6) Day, J. W.; Boesch, D. F.; Clairain, E. J.; Kemp, G. P.; Laska, S. B.; Mitsch, W. J.; Orth, K.;  
4 542 Mashriqui, H.; Reed, D. J.; Shabman, L.; Simenstad, C. A.; Streever, B. J.; Twilley, R. R.;  
5 543 Watson, C. C.; Wells, J. T.; Whigham, D. F. Restoration of the Mississippi Delta: Lessons  
6 544 from Hurricanes Katrina and Rita. *Science* **2007**, *315* (5819), 1679–1684.  
7 545 <https://doi.org/10.1126/science.1137030>.  
8 546 (7) Twilley, R. R.; Rivera-Monroy, V. Sediment and Nutrient Tradeoffs in Restoring Mississippi  
9 547 River Delta: Restoration vs Eutrophication. *J. Contemp. Water Res. Educ.* **2009**, *141* (1), 39–  
10 548 44. <https://doi.org/10.1111/j.1936-704X.2009.00035.x>.  
11 549 (8) Foufoula-Georgiou, E.; Syvitski, J.; Paola, C.; Hoanh, C. T.; Tuong, P.; Vörösmarty, C.;  
12 550 Kremer, H.; Brondizio, E.; Saito, Y.; Twilley, R. International Year of Deltas 2013: A Proposal.  
13 551 *Eos Trans. Am. Geophys. Union* **2011**, *92* (40), 340–341.  
14 552 <https://doi.org/10.1029/2011EO400006>.  
15 553 (9) DeLaune, R. D.; Kongchum, M.; White, J. R.; Jugsujinda, A. Freshwater Diversions as an  
16 554 Ecosystem Management Tool for Maintaining Soil Organic Matter Accretion in Coastal  
17 555 Marshes. *CATENA* **2013**, *107*, 139–144. <https://doi.org/10.1016/j.catena.2013.02.012>.  
18 556 (10) Twilley, R. R.; Day, J. W.; Bevington, A. E.; Castañeda-Moya, E.; Christensen, A.; Holm,  
19 557 G.; Heffner, L. R.; Lane, R.; McCall, A.; Aarons, A.; Li, S.; Freeman, A.; Rovai, A. S.  
20 558 Ecogeomorphology of Coastal Deltaic Floodplains and Estuaries in an Active Delta: Insights  
21 559 from the Atchafalaya Coastal Basin. *Estuar. Coast. Shelf Sci.* **2019**, *227*, 106341.  
22 560 <https://doi.org/10.1016/j.ecss.2019.106341>.  
23 561 (11) Bevington, A. E.; Twilley, R. R. Island Edge Morphodynamics along a Chronosequence in  
24 562 a Prograding Deltaic Floodplain Wetland. *J. Coast. Res.* **2018**, *34* (4), 806–817.  
25 563 <https://doi.org/10.2112/JCOASTRES-D-17-00074.1>.  
26 564 (12) Wagner, W.; Lague, D.; Mohrig, D.; Passalacqua, P.; Shaw, J.; Moffett, K. Elevation  
27 565 Change and Stability on a Prograding Delta. *Geophys. Res. Lett.* **2017**, *44* (4), 1786–1794.  
28 566 <https://doi.org/10.1002/2016GL072070>.  
29 567 (13) Jensen, D.; Cavanaugh, K. C.; Simard, M.; Christensen, A.; Rovai, A.; Twilley, R.  
30 568 Aboveground Biomass Distributions and Vegetation Composition Changes in Louisiana's  
31 569 Wax Lake Delta. *Estuar. Coast. Shelf Sci.* **2021**, *250*, 107139.  
32 570 <https://doi.org/10.1016/j.ecss.2020.107139>.  
33 571 (14) Carle, M. V.; Wang, L.; Sasser, C. E. Mapping Freshwater Marsh Species Distributions  
34 572 Using WorldView-2 High-Resolution Multispectral Satellite Imagery. *Int. J. Remote Sens.*  
35 573 **2014**, *35* (13), 4698–4716. <https://doi.org/10.1080/01431161.2014.919685>.  
36 574 (15) Upreti, K.; Maiti, K.; Rivera-Monroy, V. H. Microbial Mediated Sedimentary Phosphorus  
37 575 Mobilization in Emerging and Eroding Wetlands of Coastal Louisiana. *Sci Total Env.* **2019**,  
38 576 *651* (Pt 1), 122–133. <https://doi.org/10.1016/j.scitotenv.2018.09.031>.  
39 577 (16) Upreti, K.; Rivera-Monroy, V. H.; Maiti, K.; Giblin, A. E.; Castañeda-Moya, E. Dissimilatory  
40 578 Nitrate Reduction to Ammonium (DNRA) Is Marginal Relative to Denitrification in Emerging-  
41 579 Eroding Wetlands in a Subtropical Oligohaline and Eutrophic Coastal Delta. *Sci. Total*  
42 580 *Environ.* **2022**, *819*, 152942. <https://doi.org/10.1016/j.scitotenv.2022.152942>.  
43 581 (17) Shields, M. R.; Bianchi, T. S.; Gélinas, Y.; Allison, M. A.; Twilley, R. R. Enhanced  
44 582 Terrestrial Carbon Preservation Promoted by Reactive Iron in Deltaic Sediments. *Geophys.*  
45 583 *Res. Lett.* **2016**, *43* (3), 1149–1157. <https://doi.org/10.1002/2015gl067388>.  
46 584 (18) Coward, E. K.; Thompson, A. T.; Plante, A. F. Iron-Mediated Mineralogical Control of  
47 585 Organic Matter Accumulation in Tropical Soils. *Geoderma* **2017**, *306*, 206–216.  
48 586 <https://doi.org/10.1016/j.geoderma.2017.07.026>.  
49 587 (19) Lalonde, K.; Mucci, A.; Oullet, A.; Gélinas, Y. Preservation of Organic Matter in Sediments  
50 588 Promoted by Iron. *Nature* **2012**, *483*, 198–200. <https://doi.org/10.1038/nature10855>.  
51 589 (20) Reddy, K. R.; DeLaune, R. D.; Inglett, P. W. *Biogeochemistry of Wetlands: Science and*  
52 590 *Applications*, 2nd ed.; CRC Press: Boca Raton, 2022.  
53 591 <https://doi.org/10.1201/9780429155833>.

- 592 (21) Sharma, N.; Wang, Z.; Catalano, J. G.; Giammar, D. E. Dynamic Responses of Trace  
593 Metal Bioaccessibility to Fluctuating Redox Conditions in Wetland Soils and Stream  
594 Sediments. *ACS Earth Space Chem.* **2022**, *6* (5), 1331–1344.  
595 <https://doi.org/10.1021/acsearthspacechem.2c00031>.
- 596 (22) Kleber, M.; Eusterhues, K.; Keiluweit, M.; Mikutta, C.; Mikutta, R.; Nico, P. S. Mineral-  
597 Organic Associations: Formation, Properties, and Relevance in Soil Environments; Advances  
598 in Agronomy; Elsevier, 2015; Vol. 130, pp 1–420.
- 599 (23) Lützow, M. v.; Kögel-Knabner, I.; Ekschmitt, K.; Matzner, E.; Guggenberger, G.;  
600 Marschner, B.; Flessa, H. Stabilization of Organic Matter in Temperate Soils: Mechanisms  
601 and Their Relevance under Different Soil Conditions – a Review. *Eur. J. Soil Sci.* **2006**, *57*  
602 (4), 426–445. <https://doi.org/10.1111/j.1365-2389.2006.00809.x>.
- 603 (24) Coward, E. K.; Ohno, T.; Plante, A. F. Adsorption and Molecular Fractionation of Dissolved  
604 Organic Matter on Iron-Bearing Mineral Matrices of Varying Crystallinity. *Environ. Sci.*  
605 *Technol.* **2018**, *52* (3), 1036–1044. <https://doi.org/10.1021/acs.est.7b04953>.
- 606 (25) Coward, E. K.; Ohno, T.; Sparks, D. L. Direct Evidence for Temporal Molecular  
607 Fractionation of Dissolved Organic Matter at the Iron Oxyhydroxide Interface. *Environ. Sci.*  
608 *Technol.* **2019**, *53* (2), 642–650. <https://doi.org/10.1021/acs.est.8b04687>.
- 609 (26) Herndon, E.; AlBashaireh, A.; Singer, D.; Roy Chowdhury, T.; Gu, B.; Graham, D.  
610 Influence of Iron Redox Cycling on Organo-Mineral Associations in Arctic Tundra Soil.  
611 *Geochim. Cosmochim. Acta* **2017**, *207*, 210–231. <https://doi.org/10.1016/j.gca.2017.02.034>.
- 612 (27) Herndon, E. M.; Kinsman-Costello, L.; Duroe, K. A.; Mills, J.; Kane, E. S.; Sebestyen, S.  
613 D.; Thompson, A. A.; Wulschleger, S. D. Iron (Oxyhydr)Oxides Serve as Phosphate Traps in  
614 Tundra and Boreal Peat Soils. *J. Geophys. Res. Biogeosciences* **2019**, *124* (2), 227–246.  
615 <https://doi.org/10.1029/2018jg004776>.
- 616 (28) Bhattacharyya, A.; Campbell, A. N.; Tfaily, M. M.; Lin, Y.; Kukkadapu, R. K.; Silver, W. L.;  
617 Nico, P. S.; Pett-Ridge, J. Redox Fluctuations Control the Coupled Cycling of Iron and Carbon  
618 in Tropical Forest Soils. *Environ. Sci. Technol.* **2018**, *52* (24), 14129–14139.  
619 <https://doi.org/10.1021/acs.est.8b03408>.
- 620 (29) NOAA. National Climatic Data Center, Morgan City, LA Station.
- 621 (30) Davidson, R. A. *Wax Lake Outlet Control Structure Louisiana: Hydraulic Model*  
622 *Investigation*; Technical Report HL-88-23; US Army Corps of Engineers: Vicksburg, MS,  
623 1988.
- 624 (31) Kim, W.; Mohrig, D.; Twilley, R.; Paola, C.; Parker, G. Is It Feasible to Build New Land in  
625 the Mississippi River Delta? *Eos Trans. Am. Geophys. Union* **2009**, *90* (42), 373–374.  
626 <https://doi.org/10.1029/2009EO420001>.
- 627 (32) Fichot, C. G.; Harringmeyer, J.; Weiser, M. Delta-X: In Situ Water Quality Indicators across  
628 MRD, LA, USA, 2021, Version 2, 2022. <https://doi.org/10.3334/ORNLDAAAC/2080>.
- 629 (33) Roberts, H. H. *Atchafalaya-Wax Lake Deltas: The New Regressive Phase of the*  
630 *Mississippi River Delta Complex*; Sneider, John., Louisiana Geological Survey., Gulf Coast  
631 Association of Geological Societies., Louisiana State University (Baton Rouge, La. ), Series  
632 Eds.; Louisiana State University, Louisiana Geological Survey, 2003.
- 633 (34) Allen, Y. C.; Couvillion, B. R.; Barras, J. A. Using Multitemporal Remote Sensing Imagery  
634 and Inundation Measures to Improve Land Change Estimates in Coastal Wetlands. *Estuaries*  
635 *Coasts* **2012**, *35* (1), 190–200. <https://doi.org/10.1007/s12237-011-9437-z>.
- 636 (35) Twilley, R.; Fontenot-Cassaway, A.; Rovai, A. Delta-X: Feldspar Sediment Accretion  
637 Measurements, MRD, LA, USA, 2019-2023, Version 3, 2023, 0 MB.  
638 <https://doi.org/10.3334/ORNLDAAAC/2290>.
- 639 (36) Shields, M. R.; Bianchi, T. S.; Mohrig, D.; Hutchings, J. A.; Kenney, W. F.; Kolker, A. S.;  
640 Curtis, J. H. Carbon Storage in the Mississippi River Delta Enhanced by Environmental  
641 Engineering. *Nat. Geosci.* **2017**, *10*, 846–851. <https://doi.org/10.1038/ngeo3044>.

- 642 (37) Shaw, J. B.; Mohrig, D.; Whitman, S. K. The Morphology and Evolution of Channels on  
643 the Wax Lake Delta, Louisiana, USA. *J. Geophys. Res. Earth Surf.* **2013**, *118* (3), 1562–1584.  
644 <https://doi.org/10.1002/jgrf.20123>.
- 645 (38) Shaw, J. B.; Mohrig, D. The Importance of Erosion in Distributary Channel Network  
646 Growth, Wax Lake Delta, Louisiana, USA. *Geology* **2014**, *42* (1), 31–34.  
647 <https://doi.org/10.1130/G34751.1>.
- 648 (39) Holm, G. O.; Sasser, C. E. Differential Salinity Response between Two Mississippi River  
649 Subdeltas: Implications for Changes in Plant Composition. *Estuaries* **2001**, *24* (1), 78–89.  
650 <https://doi.org/10.2307/1352815>.
- 651 (40) Shaffer, G. P.; Sasser, C. E.; Gosselink, J. G.; Rejmanek, M. Vegetation Dynamics in the  
652 Emerging Atchafalaya Delta, Louisiana, USA. *J. Ecol.* **1992**, *80* (4), 677–687.  
653 <https://doi.org/10.2307/2260859>.
- 654 (41) Ma, H.; Larsen, L. G.; Wagner, R. W. Ecogeomorphic Feedbacks That Grow Deltas. *J.*  
655 *Geophys. Res. Earth Surf.* **2018**, *123* (12), 3228–3250.  
656 <https://doi.org/10.1029/2018JF004706>.
- 657 (42) Olliver, E. A.; Edmunds, D. A. Defining the Ecogeomorphic Succession of Land Building  
658 for Freshwater, Intertidal Wetlands in Wax Lake Delta, Louisiana. *Estuar. Coast. Shelf Sci.*  
659 **2017**, *196*, 45–57. <https://doi.org/10.1016/j.ecss.2017.06.009>.
- 660 (43) Carle, M. Spatial Structure and Dynamics of the Plant Communities in a Pro-grading River  
661 Delta: Wax Lake Delta. Atchafalaya Bay, LA. Doctoral Thesis, Louisiana State University,  
662 2013.
- 663 (44) Poulton, S. W.; Canfield, D. E. Development of a Sequential Extraction Procedure for Iron:  
664 Implications for Iron Partitioning in Continentally Derived Particulates. *Chem. Geol.* **2005**, *214*  
665 (3), 209–221. <https://doi.org/10.1016/j.chemgeo.2004.09.003>.
- 666 (45) Herndon, E.; Kinsman-Costello, L.; Di Domenico, N.; Duroe, K.; Barczok, M.; Smith, C.;  
667 Wulschleger, S. D. Iron and Iron-Bound Phosphate Accumulate in Surface Soils of Ice-  
668 Wedge Polygons in Arctic Tundra. *Environ. Sci. Process. Impacts* **2020**, *22* (7), 1475–1490.  
669 <https://doi.org/10.1039/d0em00142b>.
- 670 (46) APHA. 3500-Fe IRON. In *Standard Methods For the Examination of Water and*  
671 *Wastewater*; Standard Methods for the Examination of Water and Wastewater; American  
672 Public Health Association, 2017. <https://doi.org/10.2105/SMWW.2882.055>.
- 673 (47) R Core Team. R: A Language and Environment for Statistical Computing, 2023.  
674 <https://www.R-project.org/>.
- 675 (48) Wickham, H. *Ggplot2: Elegant Graphics for Data Analysis*; Springer-Verlag New York,  
676 2016.
- 677 (49) Castañeda-Moya, E.; Solohin, E. Delta-X: Soil Properties for Herbaceous Wetlands, MRD,  
678 Louisiana, 2021, V3, 2023. <https://doi.org/10.3334/ORNLDAAAC/2239>.
- 679 (50) Ma, H.; Thompson, A.; Hall, S. J.; Wang, J.; Xiao, Y.; Liu, C.-Q.; Chen, C. Enrichment of  
680 Metastable Iron Minerals in Global Coastal Wetlands. *Nat. Geosci.* **2025**.  
681 <https://doi.org/10.1038/s41561-025-01764-7>.
- 682 (51) Thompson, A.; Chadwick, O. A.; Rancourt, D. G.; Chorover, J. Iron-Oxide Crystallinity  
683 Increases during Soil Redox Oscillations. *Geochim. Cosmochim. Acta* **2006**, *70* (7), 1710–  
684 1727. <https://doi.org/10.1016/j.gca.2005.12.005>.
- 685 (52) Lin, Y.; Campbell, A. N.; Bhattacharyya, A.; DiDonato, N.; Thompson, A. M.; Tfaily, M. M.;  
686 Nico, P. S.; Silver, W. L.; Pett-Ridge, J. Differential Effects of Redox Conditions on the  
687 Decomposition of Litter and Soil Organic Matter. *Biogeochemistry* **2021**, *154* (1), 1–15.  
688 <https://doi.org/10.1007/s10533-021-00790-y>.
- 689 (53) Reddy, K. R.; Patrick, W. H. Effect of Alternate Aerobic and Anaerobic Conditions on  
690 Redox Potential, Organic Matter Decomposition and Nitrogen Loss in a Flooded Soil. *Soil*  
691 *Biol. Biochem.* **1975**, *7* (2), 87–94. [https://doi.org/10.1016/0038-0717\(75\)90004-8](https://doi.org/10.1016/0038-0717(75)90004-8).

- 692 (54) Crane, J. H.; Davies, F. S. Periodic and Seasonal Flooding Effects on Survival, Growth,  
693 and Stomatal Conductance of Young Rabbiteye Blueberry Plants. *J. Am. Soc. Hort. Sci.*  
694 **1988**, *113* (4), 488–493. <https://doi.org/10.21273/JASHS.113.4.488>.
- 695 (55) Ballantine, K. A.; Groffman, P. M.; Lehmann, J.; Schneider, R. L. Stimulating Nitrate  
696 Removal Processes of Restored Wetlands. *Environ. Sci. Technol.* **2014**, *48* (13), 7365–7373.  
697 <https://doi.org/10.1021/es500799v>.
- 698 (56) Kirwan, M. L.; Langley, J. A.; Guntenspergen, G. R.; Megonigal, J. P. The Impact of Sea-  
699 Level Rise on Organic Matter Decay Rates in Chesapeake Bay Brackish Tidal Marshes.  
700 *Biogeosciences* **2013**, *10* (3), 1869–1876. <https://doi.org/10.5194/bg-10-1869-2013>.
- 701 (57) Stagg, C. L.; Schoolmaster, D. R.; Krauss, K. W.; Cormier, N.; Conner, W. H. Causal  
702 Mechanisms of Soil Organic Matter Decomposition: Deconstructing Salinity and Flooding  
703 Impacts in Coastal Wetlands. *Ecology* **2017**, *98* (8), 2003–2018.  
704 <https://doi.org/10.1002/ecy.1890>.
- 705 (58) Herndon, E.; Berens, M. J.; Pilla, R. M.; Schwaner, G. Temporal Patterns in Soil Redox  
706 Potential Vary Across a Freshwater Coastal Delta. *Hydrol. Process.* **2025**, *39* (11), e70338.  
707 <https://doi.org/10.1002/hyp.70338>.
- 708 (59) Thompson, A.; Chadwick, O. A.; Boman, S.; Chorover, J. Colloid Mobilization During Soil  
709 Iron Redox Oscillations. *Environ. Sci. Technol.* **2006**, *40* (18), 5743–5749.  
710 <https://doi.org/10.1021/es061203b>.
- 711 (60) Chapman, S. K.; Hayes, M. A.; Kelly, B.; Langley, J. A. Exploring the Oxygen Sensitivity  
712 of Wetland Soil Carbon Mineralization. *Biol. Lett.* **2019**, *15*, 20180407.  
713 <https://doi.org/10.1098/rsbl.2018.0407>.
- 714 (61) Boye, K.; Herrmann, A. M.; Schaefer, M. V.; Tfaily, M. M.; Fendorf, S. Discerning  
715 Microbially Mediated Processes During Redox Transitions in Flooded Soils Using Carbon and  
716 Energy Balances. *Front. Environ. Sci.* **2018**, *6*, 15. <https://doi.org/10.3389/fenvs.2018.00015>.
- 717 (62) Dunham-Cheatham, S. M.; Zhao, Q.; Obrist, D.; Yang, Y. Unexpected Mechanism for  
718 Glucose-Primed Soil Organic Carbon Mineralization under an Anaerobic–Aerobic Transition.  
719 *Geoderma* **2020**, *376*, 114535. <https://doi.org/10.1016/j.geoderma.2020.114535>.
- 720 (63) Chen, C.; Hall, S. J.; Coward, E.; Thompson, A. Iron-Mediated Organic Matter  
721 Decomposition in Humid Soils Can Counteract Protection. *Nat. Commun.* **2020**, *11* (1), 2255.  
722 <https://doi.org/10.1038/s41467-020-16071-5>.
- 723 (64) Xu, Z.; Tsang, D. C. W. Mineral-Mediated Stability of Organic Carbon in Soil and Relevant  
724 Interaction Mechanisms. *Eco-Environ. Health* **2024**, *3* (1), 59–76.  
725 <https://doi.org/10.1016/j.eehl.2023.12.003>.
- 726 (65) Patzner, M. S.; Mueller, C. W.; Malusova, M.; Baur, M.; Nikeleit, V.; Scholten, T.;  
727 Hoeschen, C.; Byrne, J. M.; Borch, T.; Kappler, A.; Bryce, C. Iron Mineral Dissolution  
728 Releases Iron and Associated Organic Carbon during Permafrost Thaw. *Nat. Commun.* **2020**,  
729 *11* (1), 6329. <https://doi.org/10.1038/s41467-020-20102-6>.
- 730 (66) Shields, M. R.; Bianchi, T. S.; Kolker, A. S.; Kenney, W. F.; Mohrig, D.; Osborne, T. Z.;  
731 Curtis, J. H. Factors Controlling Storage, Sources, and Diagenetic State of Organic Carbon  
732 in a Prograding Subaerial Delta: Wax Lake Delta, Louisiana. *J. Geophys. Res.*  
733 *Biogeosciences* **2019**, *124* (5), 1115–1131. <https://doi.org/10.1029/2018JG004683>.
- 734 (67) Krauss, K. W.; Doyle, T. W.; Twilley, R. R.; Rivera-Monroy, V. H.; Sullivan, J. K. Evaluating  
735 the Relative Contributions of Hydroperiod and Soil Fertility on Growth of South Florida  
736 Mangroves. *Hydrobiologia* **2006**, *569* (1), 311–324. <https://doi.org/10.1007/s10750-006-0139-7>.
- 737 (68) Conroy, B. M.; Kelleway, J. J.; Rogers, K. Root Productivity Contributes to Carbon Storage  
738 and Surface Elevation Adjustments in Coastal Wetlands. *Plant Soil* **2025**, *513* (1), 605–631.  
739 <https://doi.org/10.1007/s11104-025-07204-0>.
- 740 (69) Kristensen, E.; Connolly, R. M.; Otero, X. L.; Marchand, C.; Ferreira, T. O.; Rivera-Monroy,  
741 V. H. Biogeochemical Cycles: Global Approaches and Perspectives. In *Mangrove*



- 794 (86) Holford, I. C. R.; Patrick, W. H. Effects of Reduction and pH Changes on Phosphate  
795 Sorption and Mobility in an Acid Soil. *Soil Sci. Soc. Am. J.* **1979**, *43* (2), 292–297.  
796 <https://doi.org/10.2136/sssaj1979.03615995004300020010x>.
- 797 (87) Stenberg, B.; Johansson, M.; Pell, M.; Sjö Dahl-Svensson, K.; Stenström, J.; Torstensson,  
798 L. Microbial Biomass and Activities in Soil as Affected by Frozen and Cold Storage. *Soil Biol.*  
799 *Biochem.* **1998**, *30* (3), 393–402. [https://doi.org/10.1016/S0038-0717\(97\)00125-9](https://doi.org/10.1016/S0038-0717(97)00125-9).
- 800 (88) Sebaaly, A. P.; Van Rijn, F.; Hanna, K.; Boily, J.-F. Ice as a Kinetic and Mechanistic Driver  
801 of Oxalate-Promoted Iron Oxyhydroxide Dissolution. *Proc. Natl. Acad. Sci.* **2025**, *122* (35),  
802 e2507588122. <https://doi.org/10.1073/pnas.2507588122>.
- 803 (89) Jeong, D.; Kim, K.; Choi, W. Accelerated Dissolution of Iron Oxides in Ice. *Atmospheric*  
804 *Chem. Phys.* **2012**, *12* (22), 11125–11133. <https://doi.org/10.5194/acp-12-11125-2012>.
- 805 (90) Goberna, M.; Insam, H.; Pascual, J. A.; Sánchez, J. Storage Effects on the Community  
806 Level Physiological Profiles of Mediterranean Forest Soils. *Soil Biol. Biochem.* **2005**, *37* (1),  
807 173–178. <https://doi.org/10.1016/j.soilbio.2004.06.014>.
- 808 (91) Peoples, M. S.; Koide, R. T. Considerations in the Storage of Soil Samples for Enzyme  
809 Activity Analysis. *Appl. Soil Ecol.* **2012**, *62*, 98–102.  
810 <https://doi.org/10.1016/j.apsoil.2012.08.002>.
- 811 (92) Hu, M.; Yan, R.; Wu, H.; Ni, R.; Zhang, D.; Zou, S. Linking Soil Phosphorus Availability  
812 and Phosphatase Functional Genes to Coastal Marsh Erosion: Implications for Nutrient  
813 Cycling and Wetland Restoration. *Sci. Total Environ.* **2023**, *898*, 165559.  
814 <https://doi.org/10.1016/j.scitotenv.2023.165559>.
- 815 (93) Nannipieri, P.; Giagnoni, L.; Landi, L.; Renella, G. Role of Phosphatase Enzymes in Soil.  
816 In *Phosphorus in Action: Biological Processes in Soil Phosphorus Cycling*; Bünemann, E.,  
817 Oberson, A., Frossard, E., Eds.; Soil Biology; Springer: Berlin, Heidelberg, 2011; pp 215–243.  
818 [https://doi.org/10.1007/978-3-642-15271-9\\_9](https://doi.org/10.1007/978-3-642-15271-9_9).
- 819 (94) Bernhardt, E. S.; Blaszczyk, J. R.; Ficken, C. D.; Fork, M. L.; Kaiser, K. E.; Seybold, E. C.  
820 Control Points in Ecosystems: Moving Beyond the Hot Spot Hot Moment Concept.  
821 *Ecosystems* **2017**, *20* (4), 665–682. <https://doi.org/10.1007/s10021-016-0103-y>.
- 822 (95) Patel, K. F.; Malhotra, A.; Norris, C. G.; McKeever, S. A.; Fields, D. M.; Musci, J. I.;  
823 Bandopadhyay, S.; Bond-Lamberty, B.; Chen, X.; Day, D. J.; Doro, K. O.; Fluet-Chouinard,  
824 E.; Garcia, M.; Kemner, K. M.; Machado-Silva, F.; McDowell, N.; Morris, K. A.; Myers-Pigg,  
825 A.; O'Loughlin, E. J.; O'Meara, T.; Peixoto, R. B.; Pennington, S. C.; Regier, P.; Rich, R.; Rod,  
826 K. A.; Sulman, B.; Thornton, P.; Ward, N.; Wilson, S. J.; Weintraub, M. N.; Magonigal, J. P.;  
827 Bailey, V. L. Transition Zones at the Changing Coastal Terrestrial-Aquatic Interface. *J.*  
828 *Geophys. Res. Biogeosciences* **2025**, *130* (11), e2025JG008978.  
829 <https://doi.org/10.1029/2025JG008978>.
- 830 (96) Thompson, A.; Rancourt, D. G.; Chadwick, O. A.; Chorover, J. Iron Solid-Phase  
831 Differentiation along a Redox Gradient in Basaltic Soils. *Geochim. Cosmochim. Acta* **2011**,  
832 *75* (1), 119–133. <https://doi.org/10.1016/j.gca.2010.10.005>.
- 833 (97) Yu, C.; Xie, S.; Song, Z.; Xia, S.; Åström, M. E. Biogeochemical Cycling of Iron (Hydr-  
834 )Oxides and Its Impact on Organic Carbon Turnover in Coastal Wetlands: A Global Synthesis  
835 and Perspective. *Earth-Sci. Rev.* **2021**, *218*. <https://doi.org/10.1016/j.earscirev.2021.103658>.
- 836

**Data availability**

The raw data supporting this article have been included as part of the Supplementary Information.

1  
2  
3  
4  
5  
6  
7  
8  
9  
10  
11  
12  
13  
14  
15  
16  
17  
18  
19  
20  
21  
22  
23  
24  
25  
26  
27  
28  
29  
30  
31  
32  
33  
34  
35  
36  
37  
38  
39  
40  
41  
42  
43  
44  
45  
46  
47  
48  
49  
50  
51  
52  
53  
54  
55  
56  
57  
58  
59  
60

Open Access Article. Published on 06 May 2022. Downloaded on 5/7/2022 6:46:05 PM.  
This article is licensed under a Creative Commons Attribution-NonCommercial 3.0 Unported Licence.



Environmental Science: Processes & Impacts Accepted Manuscript